INTERNATIONAL JOURNAL OF PROGRESSIVE RESEARCH IN ENGINEERING MANAGEMENT AND SCIENCE (IJPREMS)

e-ISSN : 2583-1062

Impact Factor: 5.725

www.ijprems.com
editor@ijprems.com

Vol. 04, Issue 07, July 2024, pp: 1344-1351

GREEN SYNTHESIS OF ZINC OXIDE NANOPARTICLES USING BAUHINIA VARIEGATA LEAVES FOR EFFECTIVE PHOTOCATALYTIC DEGRADATION OF DYES IN AQUEOUS SOLUTION AND ANTIMICROBIAL ACTIVITIES

Penmethsa Kiran Kumar[1], Janapareddi Laxmi Mangamma[2], Golthi Venkatesh[3]

[1,2,3]Lecturer in Chemistry, Department of Chemistry, Government Degree College, Chodavaram, Andhra Pradesh, India.

DOI: https://www.doi.org/10.58257/IJPREMS35588

ABSTRACT

Zinc oxide nanoparticles (ZnO-NPs) were synthesized using Bauhinia variegata (BV) leaf extract through a facile and eco-friendly green synthesis approach. The green-synthesized BV-ZnO NPs were characterized using UV-visible spectroscopy, PXRD, FT-IR, SEM, SEM-EDX, TEM, and SAED. The obtained NPs were spherical and polycrystalline with a crystallite size of 28 nm. BV-ZnO NPs were employed as photocatalysts for the degradation of three dyes, Rhodamine B (RhB), Crystal Violet (CV), and Fluorescein Sodium (FS), from aqueous solutions in sunlight. Photocatalytic degradation of 84.81% of CV dye, 94.82% of FS dye, and 91.54% of RhB dye was achieved in 30 minutes for the CV and FS dyes, whereas it took 180 minutes for the RhB dye. Antimicrobial activity was evaluated using the bacterial strains, gram-positive Staphylococcus aureus, and gram-negative Klebsiella pneumoniae. The study provided a low-cost method for removing hazardous dyes in aqueous solutions using green synthesized ZnO nanoparticles as a photocatalyst.

Keywords: Photocatalysis, removal of dyes, green synthesis, nanoparticles, Zinc oxide

1. INTRODUCTION

The impact of dyes on the environment is a critical issue that has garnered significant attention due to the pervasive use of dyes in various industries, particularly in textiles, paper, leather, and cosmetics. One of the most significant environmental impacts of dyes is water pollution. Dyes are often discharged into water bodies from industrial effluents without adequate treatment. Many dyes and their breakdown products are carcinogenic, mutagenic, or teratogenic, posing serious health risks to fish and other aquatic animals. The bioaccumulation of these toxic substances in the food chain can also affect higher trophic levels, including humans who consume contaminated fish and seafood. The presence of dyes in water bodies can block sunlight penetration, disrupting photosynthesis in aquatic plants and affecting the entire aquatic ecosystem. It is essential to devise and execute sustainable solutions that safeguard both our ecosystems and health from the threat posed by hazardous dyes present in aqueous solutions [1-3].

Traditional methods for dye removal often fall short in terms of efficiency and environmental sustainability [4-6]. Photocatalysis has emerged as a promising method for removing dyes from aqueous solutions due to several inherent advantages. In recent years, the application of nanoparticles as photocatalysts for dye removal has emerged as a promising avenue. When exposed to ultraviolet or visible light, nanoparticles generate electron-hole pairs, initiating redox reactions that break down organic pollutants, including dyes, into harmless byproducts. This mechanism offers several advantages, including high efficiency, broad applicability, and the ability to operate under ambient conditions without the requirement for additional chemicals [7-9].

One of the key advantages of using nanoparticles as photocatalysts is their high surface area-to-volume ratio, which provides ample active sites for catalytic reactions. This enhanced surface area allows for better adsorption of dye molecules onto the nanoparticle surface, facilitating their subsequent degradation. Additionally, nanoparticles can be easily dispersed in aqueous solutions, ensuring uniform contact between the photocatalyst and the dye molecules, further enhancing the efficiency of the photocatalytic process.

The green synthesis of nanoparticles is a facile, environmentally friendly, and sustainable approach that offers several advantages, including biocompatibility, scalability, and cost-effectiveness. One common method of green synthesis involves utilizing plant extracts, microbial organisms, or biomolecules such as proteins and polysaccharides as reducing and stabilizing agents [10-11].

Due to its unique properties, there are many reports on the green synthesis of Zinc oxide nanoparticles using diverse plant resources. The plant extracts' content of alkaloids, amino acids, enzymes, proteins, and polysaccharides makes them effective reducing and capping agents. This simplifies the synthesis process and improves its safety, sustainability, and environmental friendliness compared to traditional physical and chemical methods.

Zinc oxide nanoparticles (ZnO NPs) have attracted significant attention for various biomedical applications due to their advantageous properties, including biocompatibility, low toxicity, and cost-effectiveness [12-13]. These nanoparticles exhibit strong biological activities and have been employed in multiple fields for their antibacterial, anticancer, antioxidant, anti-inflammatory, and wound-healing properties However, so far, green synthesis of ZnO NPs using the Bauhinia variegata leaf extract has not been reported in the literature. Bauhinia variegata, also known locally as Devakanchanamu, is native to tropical and subtropical regions [14]. Analysis of its leaf extract has revealed a diverse array of chemical compounds, such as carbohydrates, alkaloids, flavonoids, terpenoids, phenolics, tannins, and glucosides. These compounds are credited with the plant's antifungal, anticarcinogenic, antimicrobial, antidiabetic, hypoglycemic, haematinic, and anti-inflammatory properties [15].

In the present study, ZnO NPs were synthesized using the aqueous leaf extract of Bauhinia variegata. For brevity, the as-synthesized NPs are represented as BV-ZnO NPs. The formation, particle size, morphology, and crystallinity of the BV-ZnO NPs were ascertained using different spectroscopic techniques. The antimicrobial activity of BV-ZnO NPs was assessed by gram-positive Staphylococcus aureus, and gram-negative Klebsiella pneumoniae bacterial strains. The photocatalytic efficacy of the BV-ZnO NPs in dye degradation was tested using three dyes, Rhodamine B (RhB), Crystal Violet (CV), and Fluorescein Sodium (FS). The dye degradation studies in sunlight.

2. METHODOLOGY

2.1. Materials and Instrumentation

Zinc acetate (Zn $(CH_3COO)_2$. $2H_2O$), Rhodamine B (RhB), Crystal Violet (CV), and Fluorescein Sodium (FS), and ammonia were procured from Sigma Aldrich. The Bauhinia variegate leaves were collected from the botanical garden of the Government Degree College, Chodavaram.

The formation of BV-ZnO NPs was confirmed based on colour change during the synthesis and recording of the UV-visible spectra of the leaf extract and BV-ZnO NPs using a spectrophotometer (SHIMADZU UV-2450). The surface morphology was determined using scanning electron microscopy (JEOL JSM-6390LA). The elemental analysis of synthesized BV-ZnO NPs was performed via energy-dispersive X-ray spectroscopy (EDS) using an acceleration voltage of 10 kV. The crystalline properties and phase purity of BV-ZnO NPs were examined by Bruker D8 Advance diffractometer equipped with monochromatized Cu Kα radiation (λ = 1.5406 Å) Different functional groups on the surface of BV-ZnO NPs were characterized using an FTIR spectrophotometer (Agilent Cary 660) in the 400 - 4000 cm^{-1} range. The surface topography was determined by capturing the TEM images (JEOL JEM-2100). To evaluate the crystallinity of BV-ZnO NPs, a selected area electron diffraction (SAED) pattern was recorded.

2.2 Preparation of Bauhinia variegata leaf extract

1 g of Bauhinia variegata leaf powder was added to a round-bottom flask containing 100 mL of distilled water. The solution is boiled at 60 ℃ with stirring at rpm of 300 for 60 minutes. After boiling, the extract was cooled to room temperature and filtered using Whatman filter paper. The leaf extract was kept at 4 ℃ until further use.

2.3. Green Synthesis of BV-ZnO NPs

BV-ZnO NPs were synthesized following the reported procedure with some modifications [16]. 1.09 g of Zinc acetate (Zn $(CH_3COO)_2$. $2H_2O$), was dissolved in 100 mL of distilled water and sonicated for 10 minutes. The resultant solution was heated at 70 ℃ with stirring at 300 rpm for 20 minutes. Subsequently, 10 mL of leaf extract was added and the mixture was heated at 70 ℃ with stirring at rpm of 300 for 30 minutes. Following this, 1 M ammonia solution was added dropwise with stirring at 300 rpm until the pH of the solution mixture reached 12 with the change in the colour of the solution to grey. After cooling to room temperature, the grey precipitate was separated from the solution by centrifugation at 6000 rpm for 10 minutes. The obtained product was washed several times with distilled water to remove the impurities and then calcinated at 200 ℃ for 4 hours. Using a mortar and pestle, the white BV-ZnO NPs were ground into a fine powder and used as such for characterization, dye degradation, and antimicrobial studies.

2.4. Photocatalytic degradation of RhB, CV, and FS dyes using BV-ZnO NPs

The efficacy of BV-ZnO NPs as a photocatalyst in degrading RhB, CV, and FS dyes in the respective aqueous solutions was determined using sunlight as a light source. 10 mg of BV-ZnO NPs was added to each 100 mL of 1 ppm RhB, CV, and FS dye solution. After mixing the photocatalyst, the solutions were stirred at 300 rpm for 2 hours in the dark. Then by adding NaOH solution, the pH of the solutions was adjusted to 10. The photocatalyst-loaded dye solutions at pH 10 were stirred at 300 rpm and exposed to sunlight. The dye solution concentrations were determined at fixed intervals using a spectrophotometer at a λ_{max} of 555 nm, 495 nm, and 590 nm for the RhB, FS, and CV dyes, respectively. The dye degradation rate and the degradation constant were calculated using the following equations

Degradation rate (%) = $((C_0-C)/ C_0) \times 100$

INTERNATIONAL JOURNAL OF PROGRESSIVE RESEARCH IN ENGINEERING MANAGEMENT AND SCIENCE (IJPREMS)

e-ISSN : 2583-1062

Impact Factor: 5.725

www.ijprems.com

editor@ijprems.com

Vol. 04, Issue 07, July 2024, pp: 1344-1351

$\ln (C_0/C) = kt$

Here, C_0 and C denote the initial dye concentration and dye concentration at the end of degradation. k and t indicate the degradation constant and duration of sunlight exposure.

2.5. Antimicrobial studies

The antimicrobial activity of Bauhinia variegata leaf extract and BV-ZnO NPs was tested against two bacterial strains, gram-positive Staphylococcus aureus and gram-negative Klebsiella pneumoniae using the agar well diffusion method. The study involved BV-ZnO NPs and leaf extract at concentrations of 50 µg/mL, 100 µg/mL, and 150 µg/mL. Ciprofloxacin, at 5 µg/mL, was used as the positive control. Each test was performed in triplicate for both bacterial strains.

3. RESULTS AND DISCUSSION

3.1. Characterization of BV-ZnO NPs

The synthesized BV-ZnO NPs were characterized using various analytical techniques The UV-visible spectra of Bauhinia variegata leaf extract and BV-ZnO NPs are shown in Figure 1. Absorption bands at 290 nm and 338 nm were observed in the BV plant extract spectrum. These bands are attributed to the phytochemicals in the aqueous leaf extract of Bauhinia variegata. In the spectrum of BV-ZnO NPs, a characteristic peak at 369 nm was observed in the UV-visible region may be attributed to the reaction between the phytochemicals of leaf extract and Zinc salt. It closely resembled the typical UV-visible spectrum of ZnO-based NPs reported in the literature [17].

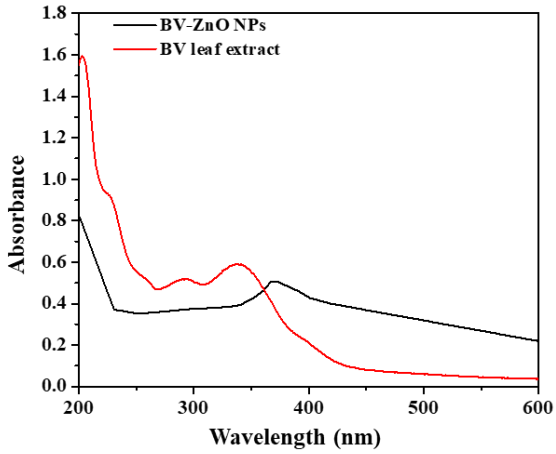

Figure 1: UV- visible spectrum of (a) Bauhinia variegata leaf extract and (b) BV-ZnO NPs

The FTIR spectra of Bauhinia variegata leaf extract and BV-ZnO NPs are presented in Figure 2. In the FTIR spectrum of the Bauhinia variegata leaf extract, the bands observed at 3306 cm^{-1} and 1632 cm^{-1} were attributed to the presence of the O-H group of phenolic compounds and the carbonyl group of carboxylic acid respectively. In the FTIR spectrum of BV-ZnO NPs, a band centred around 3359 cm^{-1} was assigned to the stretching frequency of the phenolic O-H group, likely originating from the Bauhinia variegata leaf extract. The bands at 1393 cm^{-1} and 1558 cm^{-1} were ascribed to the symmetric and asymmetric stretching vibrations of C=O bonds in the carboxylate. The peak at 1022 cm^{-1} was attributed to C-O stretching. A strong absorption band observed at 434 cm^{-1} was due to the presence of Zr-O bonds in the BV-ZnO NPs [18].

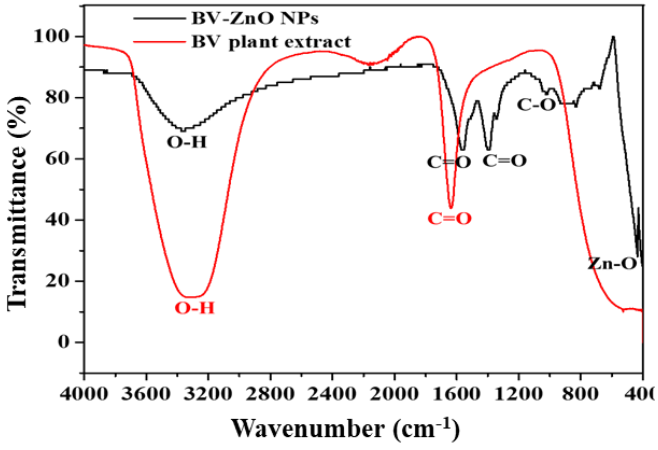

Figure 2: FT-IR spectrum of (a) Bauhinia variegata leaf extract and (b) BV-ZnO NPs

INTERNATIONAL JOURNAL OF PROGRESSIVE RESEARCH IN ENGINEERING MANAGEMENT AND SCIENCE (IJPREMS)

e-ISSN : 2583-1062

Impact Factor: 5.725

www.ijprems.com

editor@ijprems.com

Vol. 04, Issue 07, July 2024, pp: 1344-1351

In Figure 3, the PXRD patterns of the BV-ZnO NPs are displayed. Consistent with earlier studies, characteristic diffraction peaks at 2θ values of 31.88°, 34.53°, 36.34°, 47.64°, 56.72°, 62.98°, 66.46°. 68.04°, 69.19°, 72.69°, and 77.04° were observed, corresponding to the (100), (002), (101), (102). (110), (103), (200), (112), (201), (004), and (202) planes, respectively. These observed diffraction peaks were matched well with the standard PXRD patterns of ZnO NPs with wurtzite structure (JCPDS Card No. 89-0510), confirming the crystallinity of the synthesized BV-ZnO NPs [19]. The (002) peak intensity indicates that the BV-ZnO NPs are spherical.

The crystallite size of BV-ZnO NPs was calculated using the Scherrer equation.

$$D = \frac{k\lambda}{\beta_{101}\,Cos\theta_{101}}$$

Where D is the average crystallite size, k is a constant and is equal to 0.9, λ is the wavelength of X-rays (0.154 nm), β_{101} is the width (full-width at half-maximum) of the X-ray diffraction peak (in radians), and θ_{101} is the Bragg angle corresponding to the (101) plane. The mean crystallite size of BV-ZnO NPs was determined to be 28.06 nm.

For the (101) plane, the inter-planar spacing (d_{101}) was calculated using the equation

$$d_{hkl} = \frac{\lambda}{2sin\theta}$$

The value of d_{101} was calculated as 0.247 nm.

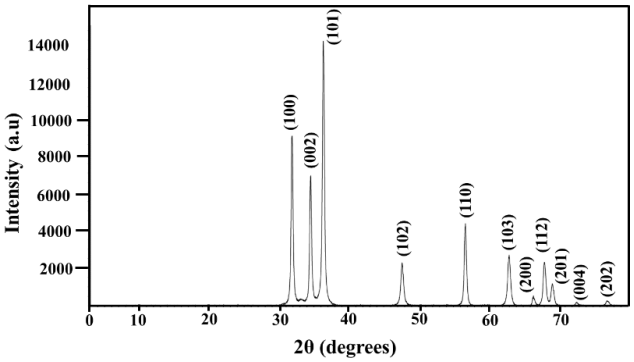

Figure 3: PXRD patterns of BV-ZnO NPs

Figure 4a shows the SEM image of BV-ZnO NPs. The nanoparticles were observed to have a spherical shape with aggregations. The EDS spectrum of BV-ZnO NPs is presented in Figure 4b. Signals at 8.630 keV (Kα line) and 1.012 keV (Lα line) confirmed the presence of Zinc and signal at 0.525 KeV (Kα line) oxygen respectively in BV-ZnO NPs. A very low-intensity signal at 0.525, corresponding to the Kα line of Carbon, is also present in the spectrum. The absence of peaks arising from other elements like Nitrogen indicates the purity of the synthesized nanoparticles. The TEM images of BV-ZnO NPs in Figures 4a and 4b show that the particles have a spherical shape. From Figure 4c, the 'd' spacing was found to be 0.230 nm, closely matching the 'd' value of 0.247 nm derived from PXRD. The selected area electron diffraction (SAED) pattern of BV-ZnO NPs is shown in Figure 4d.

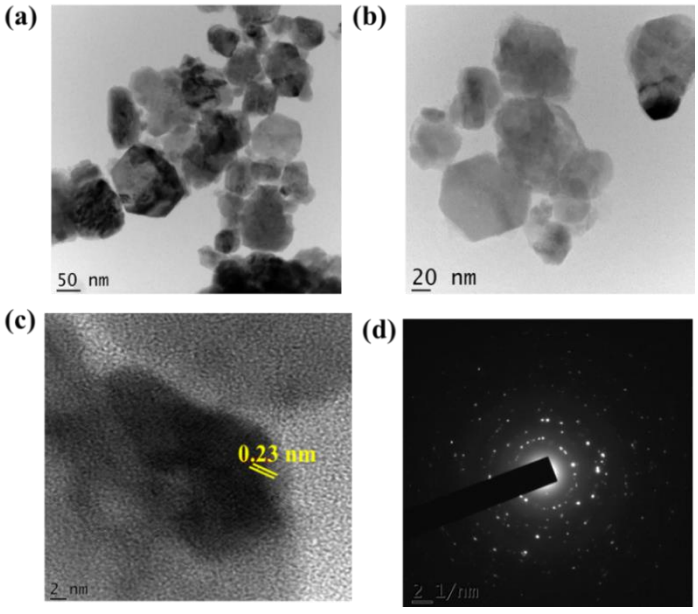

Figure 4: (a)-(c) TEM images of BV-ZnO NPs. (d) SAED patterns of BV-ZnO NPs

INTERNATIONAL JOURNAL OF PROGRESSIVE RESEARCH IN ENGINEERING MANAGEMENT AND SCIENCE (IJPREMS)

e-ISSN : 2583-1062

Impact Factor: 5.725

www.ijprems.com

editor@ijprems.com

Vol. 04, Issue 07, July 2024, pp: 1344-1351

The SAED pattern reveals concentric rings with intermittent dots, characteristic of polycrystalline nanoparticles. Using ImageJ, the average size of 50 particles in the TEM image was determined. The diameter of particles was plotted as a histogram and fitted with Gaussian distribution, as illustrated in Figure 5. The average diameter of BV-ZnO NPs was 31.44 nm, closely matching the PXRD result of 28.06 nm.

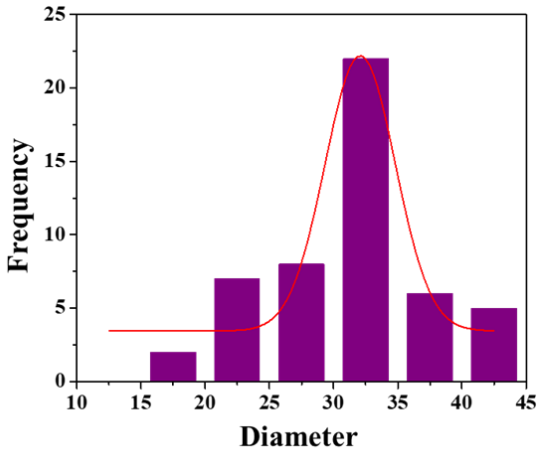

Figure 5: Particle size distribution of BV-ZnO NPs from TEM image

3.2 Mechanism for the formation of BV-ZnO NPs

The proposed mechanism for the green synthesis of BV-ZnO NPs in Figure 6 involves various phytochemicals, especially flavonoids, terpenoids, tannins, and glucosides, which act both as reducing and capping agents [20]. The chromatographic analysis identified 'quercetin', a flavonoid, as a key compound present in high concentrations in Bauhinia variegata [21]. The mechanism starts with the formation of a complex between Zn^{2+} ions and the hydroxyl groups of quercetin. This complex undergoes hydrolysis to form zinc hydroxide ($Zn(OH)_2$), which then converts to ZnO upon heating. Finally, ZnO grows through electrostatic interactions, resulting in the formation of ZnO nanoparticles.

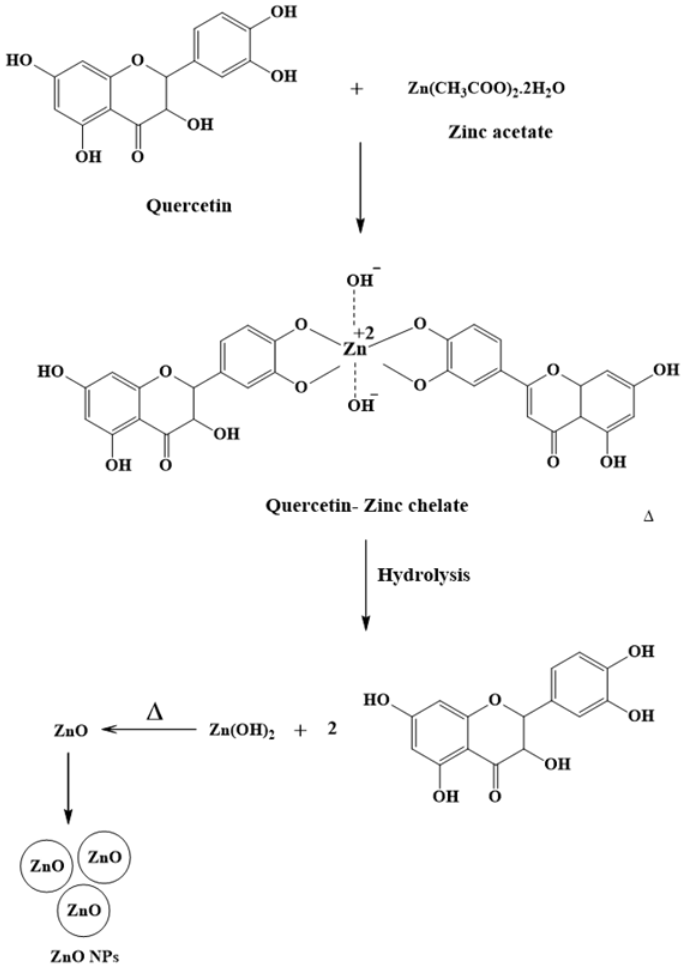

Figure 6: Mechanism for the green synthesis of BV-ZnO NPs

INTERNATIONAL JOURNAL OF PROGRESSIVE RESEARCH IN ENGINEERING MANAGEMENT AND SCIENCE (IJPREMS)

e-ISSN : 2583-1062

Impact Factor: 5.725

www.ijprems.com

editor@ijprems.com

Vol. 04, Issue 07, July 2024, pp: 1344-1351

3.3 Photocatalytic degradation of CV, FS, and RhB dyes

The degradation of CV, FS, and RhB dyes present in aqueous solutions was carried out using the BV-ZnO NPs as the photocatalyst resulting in 84.81% CV degradation in 30 minutes, 94.82 % FS degradation in 30 minutes, and 91.54% RhB degradation in 180 minutes. Figures 7, 8, and 9 illustrate the photocatalytic degradation of CV, FS, and RhB dyes monitored using the UV-visible spectrophotometer. The kinetics of CV, FS, and RhB dye degradation were best described using the Langmuir-Hinshelwood model, one of the most effective models for explaining the kinetic behavior of heterogeneous catalysis [22]. For very dilute solutions, the rate equation for Langmuir-Hinshelwood model can be expressed by the equation,

$\ln (C_0/C) = kt$

The first-order-rate constant k was determined using the slopes of the plots in Figures 7c, 8c, and 9c. k was found to be 0.06188 min^{-1}, 0.09708 min^{-1}, and 0.01434 min^{-1} for CV, FS, and RhB dyes, respectively consistent with the reported work.

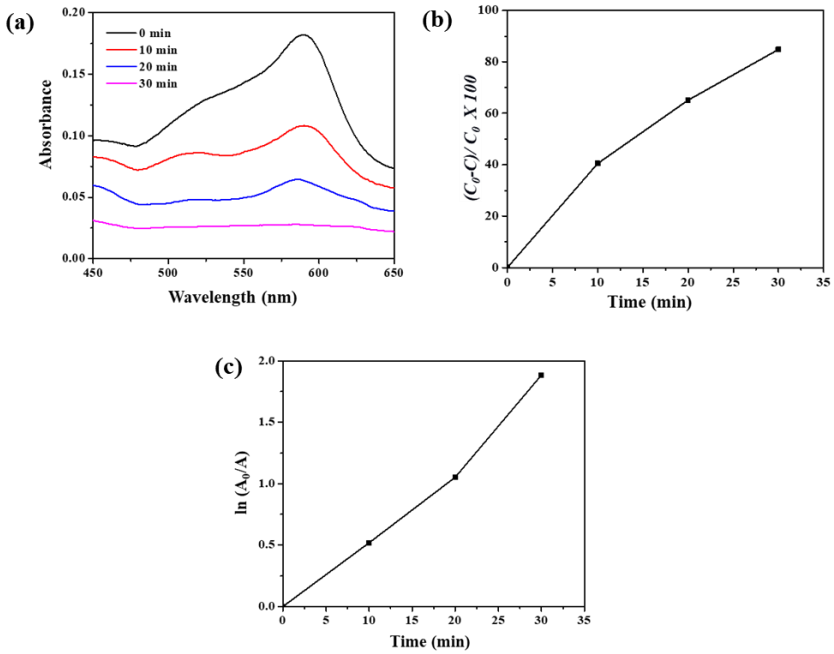

Figure 7: (a) UV-vis absorbance spectra of CV dye as a function of time over BV-ZnO NPs under sunlight (b) Percentage of CV dye degradation over time of exposure to sunlight (c) First order linear plot for CV dye degradation kinetics

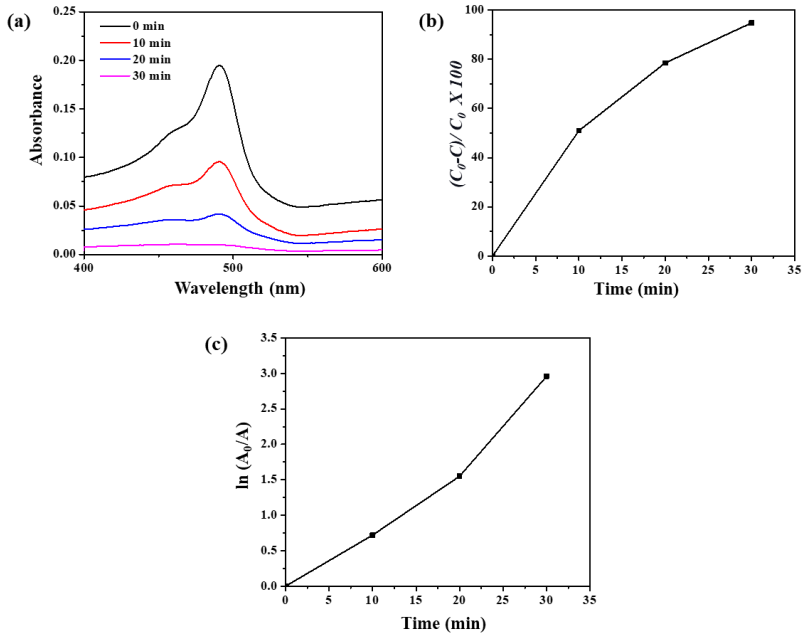

Figure 8: (a) UV-vis absorbance spectra of FS dye as a function of time over BV-ZnO NPs under sunlight (b) Percentage of FS dye degradation over time of exposure to sunlight (c) First order linear plot for FS dye degradation kinetics

INTERNATIONAL JOURNAL OF PROGRESSIVE RESEARCH IN ENGINEERING MANAGEMENT AND SCIENCE (IJPREMS)

e-ISSN : 2583-1062

Impact Factor: 5.725

www.ijprems.com

editor@ijprems.com

Vol. 04, Issue 07, July 2024, pp: 1344-1351

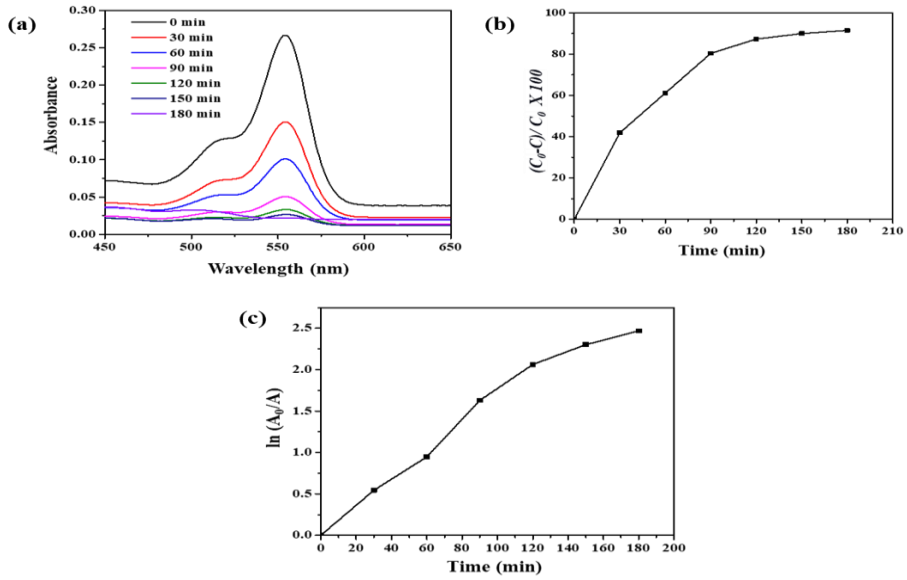

Figure 8: (a) UV-vis absorbance spectra of RhB dye as a function of time over BV-ZnO NPs under sunlight (b) Percentage of RhB dye degradation over time of exposure to sunlight (c) First order linear plot for RhB dye degradation kinetics

3.4. Antimicrobial activity

Antimicrobial studies indicated that Bauhinia variegata leaf extract has no antimicrobial effect on two bacterial strains: gram-positive Staphylococcus aureus and gram-negative Klebsiella pneumonia. The zone of inhibition values are shown in Table 1. The minimum inhibitory concentration (MIC) value of BV-ZnO NPs for both bacterial strains was 50 µg/mL, as shown in Figure 10. The study indicates that BV-ZnO NPs exhibit small to medium antimicrobial activity against bacterial strains.

Table 1. Zone of inhibition values with different concentrations of BV-ZnO NPs

Bacterial strain	Concentration of BV-ZnO NPs			Concentration of Ciprofloxacin (standard antibiotic)
	50 µg mL^{-1}	100 µg mL^{-1}	150 µg mL^{-1}	5 µg mL^{-1}
Staphylococcus aureus	11 mm	12 mm	13 mm	37 mm
Klebsiella pneumoniae	12 nm	13 mm	15 mm	40 mm

4. CONCLUSION

A green and sustainable method was employed to synthesize ZnO nanoparticles (BV-ZnO NPs) using an aqueous leaf extract of Bauhinia variegata. The synthesized BV-ZnO NPs demonstrated effective photocatalytic properties for the removal of CV and FS dyes from aqueous solutions under sunlight. The studies showed that the photodegradation process follows first-order kinetics. Additionally, the antimicrobial activity of BV-ZnO NPs was tested against gram-positive Staphylococcus aureus and gram-negative Klebsiella pneumoniae. The study underscored the potential application of green-synthesized BV-ZnO NPs in removing hazardous dyes from aqueous solutions.

ACKNOWLEDGMENTS

We are thankful to the Sophisticated Analytical Instrument Facility (SAIF) at STIC, Kochi for providing the spectral data.

5. REFERENCES

[1] Raina S, Roy A, Bharadvaja N. Degradation of dyes using biologically synthesized silver and copper nanoparticles. Environmental Nanotechnology, Monitoring & Management 2020; 13: 100278. https://doi.org/10.1016/j.enmm.2019.100278

[2] Sharma J, Sharma S, Soni V. Classification and impact of synthetic textile dyes on Aquatic Flora: A review. Regional Studies in Marine Science 2021; 45: 101802. https://doi.org/10.1016/j.rsma.2021.101802

[3] Al-Tohamy R, Ali SS, Li F, Okasha KM, Mahmoud YA et al. A critical review on the treatment of dye-containing wastewater: Ecotoxicological and health concerns of textile dyes and possible remediation approaches for environmental safety. Ecotoxicology and Environmental Safety 2022; 231: 113160. https://doi.org/10.1016/j.ecoenv.2021.113160

[4] Ruan, Wenqian, et al. "Removal of dyes from wastewater by nanomaterials: a review." Advanced Materials Letters 10.1 (2019): 9-20. https://doi.org/10.5185/amlett.2019.2148

[5] Agarwala, Rishabh, and Lavanya Mulky. "Adsorption of dyes from wastewater: A comprehensive review." ChemBioEng Reviews 10.3 (2023): 326-335. https://doi.org/10.1002/cben.202200011

[6] Panda, Sandip K., et al. "Magnetite nanoparticles as sorbents for dye removal: a review." Environmental Chemistry Letters 19 (2021): 2487-2525. https://doi.org/10.1007/s10311-020-01173-9

[7] Jara, Yohannes Shuka, Tilahun Tumiso Mekiso, and Alemayhu Pawulos Washe. "Highly efficient catalytic degradation of organic dyes using iron nanoparticles synthesized with Vernonia Amygdalina leaf extract." Scientific Reports 14.1 (2024): 6997. https://doi.org/10.1038/s41598-024-57554-5

[8] Senthil Rathi, B., et al. "Recent trends and advancement in metal oxide nanoparticles for the degradation of dyes: synthesis, mechanism, types and its application." Nanotoxicology (2024):1-27. https://doi.org/10.1080/17435390.2024.2349304

[9] Mehta, Malvika, et al. "Degradation of synthetic dyes using nanoparticles: a mini-review." Environmental Science and Pollution Research 28 (2021): 49434-49446. https://doi.org/10.1007/s11356-021-15470-5

[10] Verma R, Pathak S, Srivastava AK, Prawer S, Tomljenovic-Hanic S. ZnO nanomaterials: Green synthesis, toxicity evaluation and new insights in biomedical applications. Journal of Alloys and Compounds. 2021; 876: 160175

[11] Ying S, Guan Z, Ofoegbu PC, Clubb P, Rico C, He F, Hong J. Green synthesis of nanoparticles: Current developments and limitations. Environmental Technology & Innovation 2022; 26: 102336. https://doi.org/10.1016/j.eti.2022.102336

[12] Singh, Th Abhishek, Joydeep Das, and Parames C. Sil. "Zinc oxide nanoparticles: A comprehensive review on its synthesis, anticancer and drug delivery applications as well as health risks." Advances in colloid and interface science 286 (2020): 102317. https://doi.org/10.1016/j.cis.2020.102317

[13] Sirelkhatim, Amna, et al. "Review on zinc oxide nanoparticles: antibacterial activity and toxicity mechanism." Nano-micro letters 7 (2015): 219-242. https://doi.org/10.1007/s40820-015-0040-x

[14] Sharma K, Kumar V, Kumar S, Sharma R, Mehta CM. Bauhinia variegata: a comprehensive review on bioactive compounds, health benefits and utilization. Advances in Traditional Medicine 2021; 21: 645-653. https://doi.org/10.1007/s13596-020-00472-4

[15] Abdel-Halim AH, Fyiad AA, Aboulthana WM, El-Sammad NM, Youssef AM, Ali MM. Assessment of the anti-diabetic effect of Bauhinia variegata gold nano-extract against streptozotocin induced diabetes mellitus in rats. Journal of Applied Pharmaceutical Science 2020; 10(05): 077-91. https://dx.doi.org/10.7324/JAPS.2020.10511

[16] [16] Abdelbaky, Ahmed S., et al. "Green approach for the synthesis of ZnO nanoparticles using Cymbopogon citratus aqueous leaf extract: characterization and evaluation of their biological activities." Chemical and Biological Technologies in Agriculture 10.1 (2023): 63. https://doi.org/10.1186/s40538-023-00432-5

[17] Gawade, V. V., et al. "Green synthesis of ZnO nanoparticles by using Calotropis procera leaves for the photodegradation of methyl orange." Journal of Materials Science: Materials in Electronics 28 (2017): 14033-14039. https://doi.org/10.1007/s10854-017-7254-2

[18] Bashir, Saiqa, et al. "In-vivo (Albino Mice) and in-vitro assimilation and toxicity of zinc oxide nanoparticles in food materials." International Journal of Nanomedicine 17 (2022): 4073. https://doi.org/10.2147%2FIJN.S372343

[19] Golthi, Venkatesh, Jayarao Kommu, and A. V. Ramesh. "A green and sustainable approach to the fabrication of ZnO nanoparticles via Jatropha podagrica leaf extract for effective dye degradation and antibacterial applications." Colloid and Polymer Science 302.2 (2024):183-197. https://doi.org/10.1007/s00396-023-05187-x

[20] Xu, Jun, et al. "A review of the green synthesis of ZnO nanoparticles using plant extracts and their prospects for application in antibacterial textiles." Journal of Engineered Fibers and Fabrics 16 (2021): 15589250211046242. https://doi.org/10.1177/15589250211046242

[21] Gul, Hina, et al. "Quantification of biochemical compounds in Bauhinia Variegata Linn flower extract and its hepatoprotective effect." Saudi Journal of Biological Sciences 28.1 (2021): 247-254. https://doi.org/10.1016/j.sjbs.2020.09.056

[22] Rahman, Qazi Inamur, et al. "Synthesis and characterization of CuO rods for enhanced visible light driven dye degradation." Journal of Nanoscience and Nanotechnology 20.12 (2020): 7716-7723.https://doi.org/10.1166/jnn.2020.18713